Detection by fluorescence microscopy of N-aminopeptidases in bacteria using an ICT sensor with multiphoton excitation: Usefulness for super-resolution microscopy.

Javier Valverde-Pozo[§]; Jose M. Paredes[§]*; Carmen Salto-Giron[§]; Pilar Herrero-Foncubierta[‡]; María D. Giron[ɣ]; Delia Miguel[§]; Juan M. Cuerva[‡]; Jose M. Alvarez-Pez[§]; Rafael Salto[ɣ]; Eva M. Talavera[§]

[§] Department of Physical Chemistry, Faculty of Pharmacy, Unidad de Excelencia en Quimica Aplicada a Biomedicina y Medioambiente (UEQ), University of Granada, C. U. Cartuja, 18071 Granada, Spain.
[‡] Department of Organic Chemistry, Faculty of Sciences, Unidad de Excelencia en Quimica Aplicada a Biomedicina y Medioambiente (UEQ), University of Granada, C. U. Fuentenueva s/n, 18071, Granada, Spain.
[ɣ] Department of Biochemistry and Molecular Biology II, Faculty of Pharmacy, Unidad de Excelencia en Quimica Aplicada a Biomedicina y Medioambiente (UEQ), University of Granada, Cartuja Campus, 18071 Granada, Spain

Abstract

Bacterial proteases are relevant in pathological processes such as the survival, growth and development of microorganisms. In particular alanine amino peptidase (pepN), which is present in Gram (–) bacteria, is the only peptidase responsible for the ATP-independent degradation of cytosolic proteins in *E. coli*. These peptidases, including pepN, might be useful targets to fight bacterial infections, which are difficult to treat due to the increase in antibiotic resistance, as well as for diagnosis. In this work, we propose a new methodology for the identification of pepN-expressing bacteria by using a specific substrate, namely, DCM−NH−Ala. Substrate hydrolysis by pepN produces a sharp increase in the fluorescence band with peak at 662 nm when excited by a single photon at 480 nm or by two NIR photons (at approximately 800 nm). The emission kinetics are dependent on the intracellular pepN concentrations, which provide a powerful tool for detecting diverse virulent bacteria in a few minutes and with the inherent advantages of two-photon excitation. We resolved the enzymatic kinetics, obtained the Michaelis-Menten parameters (e.g., K_M, v_{max}, and $k_{catalytic}$) and studied the photophysics of the released fluorophore DCM−NH_2. In addition, DCM−NH_2 meets the requirements for use in super-resolution microscopy. In bacteria with high pepN activity, the probe quickly initiates an enzymatic reaction at specific sites located on the bacterial membrane and some structures inside the bacterial body.

Keywords:

Alanine amino peptidase; fluorescent sensor; bacteria; two-photon excitation; STED microscopy; bioimaging.

1. Introduction

Fluorescent probes to monitor biological activity inside living bacteria, biofilms, cells, and tissues are currently attracting much attention. From the information that fluorescence imaging methods provide, exceptional progress is being made in biological

analyses and visualization of dynamic events inside investigated organisms so that the synthesis and application of new fluorescent probes has gained significant importance [1].

A requirement that these sensors must meet is emit at red wavelengths or at near infrared wavelengths avoiding possible overlaps with the autofluorescence of the biological fluids of choice [2-6]. Moreover, to achieve deep penetration inside the interior of a living organism, it is an indispensable requisite that the incident light be of a long wavelength. For this, one can use a methodology that consists of exciting the fluorophore by absorbing two simultaneous photons with a wavelength that doubles or exceeds that needed to excite the same fluorophore with a single photon [7, 8]. This technique, which is called fluorescence microscopy by two photons (TPM), was theoretically predicted in 1931 by Maria Göppert-Meyer [9], although was not applied in fluorescence microscopy until 1990 [7]. Fluorophore excitation with NIR laser pulses provides clear advantages over excitation by a single photon of much higher energy (OPM), namely: reduced damage caused in organisms due to the lower energy of the incident radiation, lower fluorescence background from the living organism, practical absence of photobleaching by the probe, and increased depth of penetration which allows a better spatial localization of the probe in the three dimensions [10, 11].

Both the characteristics that the laser source and the TPM probes must possess have been the subject of recent research and there are several good reviews on the technical requirements and applications of two-photon microscopy [8, 10, 11]. As a general guideline, a laser with approximately 5 mW of power should be used on the objective lens, and with respect to the probes, they should have absorption cross section values equal to or greater than 50 Göppert-Mayer (GM) units. Under these conditions, bright images can be achieved by TPM without causing appreciable damage to the sample.

Recent advances in microscopy instrumentation along with the combination of different photophysical and mathematical approaches have allowed the light diffraction limit to be exceeded, which has extended the field of fluorescence microscopy to the nanometer scale. Among these techniques, the so-called STED method (Stimulated Emission Depletion), introduced by Hell and Wichmann in 1994 [12], is one of the most interesting. In this method, a de-excitation doughnut is scanned around the excitation beam and results in the confinement of excitation in some dyes and an associated improvement in resolution. The potential of super-resolution images in biological research lies not only in the possibility of visualizing nanostructures in living organisms, such as cells or bacteria, but also of contributing to the determination of the three-dimensional locations of their interactions with substructures in the organisms under study and thus can offer wider functional characterization [13, 14]. Specifically, one area in which super-resolution microscopy can be applied is obtaining location images of hot spots of catalytic activity in living structures. Since this goal requires the specific photophysical properties of the fluorescent probe [15, 16], the development of new emissive systems to study this subject is a current research topic.

Internal charge transfer (ICT)-based probes, which are obtained via conjugation of an electron donor group and an electron acceptor group within the same molecule, have been mostly used for sensing a wide variety of analytes [17, 18]. Within this type of probe, dicyanomethylene derivatives (DCM) are small chromophoric molecules that have one

broad absorption band that results from an ultrafast ICT process along with emission wavelengths in the NIR region and high photostability over a wide biological pH range. The NH_2 moiety acts as an electron-donating group, the donor characteristics of which strongly depend on amine substitution. If the electron-donating characteristics of the NH_2 moiety decrease, a shift towards shorter wavelengths in both the absorption and emission spectra, which result from a decrease in the ICT efficiency, is expected [19, 20]. The analyte-induced changes in the intensities of the two emission bands corresponding to both free and substituted DCM–NH_2 result in an effective internal reference that defines the so-called ratiometric probes that have been extensively used to improve analyte quantification. In addition, DCM–NH_2 has the additional characteristic of being a typical donor–π–acceptor (D–π–A) with a two-photon absorption cross sections of 50 GM at 820 nm in DMSO [21]. Other ratiometric two-photon fluorescent probes have recently been developed to monitor different relevant parameters in living cells and tissues [22-24].

Bacterial proteases are relevant in pathological processes since proteolysis is involved in the fundamental processes for survival, growth and development of microorganisms. In particular, the bacterial alanine amino peptidase counterpart coded by the *pepN* gene is present in Gram (–) bacteria, such as *Escherichia coli*, but not in Gram (+) bacteria [25]. *E. coli* pepN is a broad-specificity metalloaminopeptidase that is dependent on Fe and, to a lesser extent, on Zn. In *E. coli,* pepN is the only alanyl aminopeptidase responsible for the ATP-independent degradation of cytosolic proteins [26], so it is highly involved in important functions such as proteome maintenance and nutrient use.

More importantly, bacterial pathogens use proteases and peptidases to target host-specific functions [27], which is the case for the pepN protease, and it is involved in enhanced pathogenicity in *Mycobacterium tuberculosis*, probably due to its direct interaction with host macrophages [28, 29]. Furthermore, the importance of the location of pepN in the macrophage-bacteria interaction has previously been highlighted [30], which indicates the importance of a microscopy fluorescent method for detecting proteases in bacteria. In other situations, pepN can facilitate the clearance of bacterial pathogens by organisms since neutrophils are able to directly target the bacterial pepN protein to opsonize bacteria such as *Streptococcus pneumoniae* [31].

Therefore, these peptidases, including pepN, can serve as targets in the search for antimicrobial inhibitors to fight bacterial infections that are difficult to treat due to increases in antibiotic resistance [32]. Most of the inhibitors of bacterial pepN are produced by microorganisms and have been purified from cultures of these microorganisms. The most frequently used inhibitor is bestatin, which has also used as a model for studying the physiological functions of this enzyme [33]. Therefore, due to a shortage of inhibitors and the need to understand the mechanism of action of this enzyme, the use of probes that can interact with it provides a new method for studying enzyme function and may become a new diagnostic strategy to discriminate between different types of infections caused by Gram (–) bacteria [34].

Although fluorescent probes are a powerful tool for detecting protease activity [35-37] very few examples of excitation by two photons aimed at monitoring enzyme-mediated reactions are presently known. Thus, probes have been designed and synthesized to detect

the activity of phosphatase [38, 39], monoamine oxidase (MAOs) [40, 41], tyrosinase [42], cyclooxygenase-2 [43], b-galactosidase [44], leucine aminopeptidase [45], glutathione peroxidase [46] and, recently, alanine amino peptidase activity in eukaryotic cells and tissues [47] and to discriminate cancer cells during surgery [48]. Nevertheless, to the best of our knowledge, none of these probes have been used to obtain STED images in living organisms.

With these considerations in mind, we herein synthesized a pepN-specific probe by introducing an alanine moiety at the amino acid position of DCM−NH_2 that should shift both the absorption and emission spectra of the chromophore toward shorter wavelengths due to the strong effect on electron-withdrawal of the amide bond. Thus, when pepN acts on the synthesized substrate, the electron donor capacity of DCM−NH_2 will be restored and will provide a notable ratiometric fluorescence signal between the peaks of the bands from both DCM−NH_2 and the alanine derivative. After the enzymatic reaction has been described, the probe was used to develop a new methodology for the identification of Gram (−) bacteria that express pepN activity by both single-photon and multiphoton fluorescence microscopy. Finally, the usefulness of this probe for obtaining fluorescence STED images was demonstrated, and the hot spots where enzymatic reactions begin were located.

2. Experimental

2.1. Materials and methods

Unless otherwise specified, all the starting materials were commercially acquired without any further purification. The dyes DCM-NH-Ala and DCM-NH_2 were dissolved in deuterated dimethyl sulfoxide (DMSO) to obtain 0.5 mM stock solutions to verify the purity and stability of the probe by ^{1}H-NMR in the course of the experiments. All the experiments were carried out in a PBS/DMSO buffer solution (7:3, v/v) except for the solvatochromic study in which 5 µL of DCM-NH_2 was added to 1,500 µL of 12 different solvents.

2.2. Instrumentation and image processing.

The absorption spectra were obtained using a Lambda 650 UV-visible spectrophotometer (Perkin Elmer, Waltham, MA, USA). Steady-state fluorescence emission spectra and kinetics were collected on a Jasco FP-8500 spectrofluorometer (Jasco, Tokyo, Japan) that was equipped with a 150 W xenon arc lamp for excitation and R3788-01 photomultiplier tube. Both instruments were equipped with temperature controllers. Fluorescence spectra were corrected using Rhodamine 6G in EtOH as reference.

Images of the fluorescence emission intensities were obtained on a Microtime 200 fluorescence microscope system (PicoQuant GmbH, Berlin, Germany) whose excitation source consisted of a pulsed laser diode operating at λ = 375 nm. The light beam was directed onto a dichroic mirror (375 dcxr, Chroma) and then through an oil immersion objective (1.4 NA, 100×) specific to an inverted microscope system ((IX-71, Olympus, Tokyo, Japan). The fluorescence emissions were carried to a 405-nm long-pass filter (AHF/Chroma) and were focused to a 75-µm confocal pinhole. The fluorescence emissions

passed through a dichroic mirror (600 dcxr, Chroma) and were focused on single-photon avalanche diodes (SPCM-AQR 14, Perkin Elmer). The data were acquired by a TimeHarp 200 TCSPC module (PicoQuant), and raw fluorescence intensity images were obtained by a scanner at a resolution of 512 × 512 pixels. Two-photon imaging was performed using a Leica SPS II confocal microscope equipped with a Mai Tai Multiphoton laser (λ =800 nm) and an argon multiline laser (λ =458 nm). When necessary, the excitation wavelengths were sequentially switched between 800 and 458 nm and the emission bands were acquired from 500-580 and from 580-700 nm for the green and red channels, respectively. The objective used was a PL APO 63x/1.2 CS water immersion device. Fluorescence was acquired using a hybrid detector (HyD. Leica). STED and confocal images were obtained with an Abberior scanning microscope (Abberior Instruments GmbH, Germany) that was equipped with a pulsed excitation laser (485 nm, 40 MHz), and a pulsed STED laser (775 nm, 40 MHz). The objective used was an UPlanSApo 100x/1.40 oil immersion device. In all measurements, the pinhole size was set to 1 AU.

All images were exported as matrix data and were analyzed using custom macros in *Fiji is just image j* [49]. In short, the two channels were analyzed separately. First, a Gaussian blur filter (radio = 1) was applied to the raw images, and we manually set an intensity threshold by selecting bacteria in both channels. Below this threshold, the pixels were set to null values. When it was of interest, we represented the red channels by following a red/yellow/white color scale. In other cases, we calculated the ratiometric values between the red and green channels and represented these images using a blue/grey/yellow color scale.

2.3. Cloning and generation of vectors for the expression of bacterial pepN. Production and purification of the same.

The coding sequence corresponding to the *E. coli pepN* gene (Genebank adhesion # M15676.1) [50] was amplified by PCR using *Pfu* polymerase from genomic DNA from the K12 *E. coli* strain (Gene Jet Whole Blood Genomic DNA Purification Mini (Thermo Fisher, Massachusetts, USA)) using the primers pepN-f 5´-ggatccatgactcaacagccacaagcc-3´ and pepN-r 5´-gtcgacagccagtgctttagttatcttctc-3´, to which the *BamH*I and *Sal*I restriction site sequences have been added, respectively. These primers correspond to the 5´and 3´ coding sequences of the gene and for the 3´ sequence, and the nucleotides encoding the stop sequence have been removed. The amplified 2622-bp fragment was cloned in the pJET1.2 vector (Thermo Fisher), *BamH*I and *Sal*I digested and subcloned in-frame into the pMAL-TEV-His expression vector [51], which thus rendered the *pMAL-TEV-pepN-His* plasmid. The plasmid sequence was confirmed by automatic sequencing.

For the expression of the recombinant protein, XL1-Blue competent cells were transformed with the *pMAL-TEV-pepN-His* plasmid and then grown in LB media supplemented with antibiotics at 37°C until they reached OD_{600} = 0.5; the culture was then cooled to 32°C and IPTG was added to provide a final concentration of 1 mM. Growth occurred for an additional period of 12 hours at 32°C.

Upon induction, cells were harvested by centrifugation, and the cell pellets corresponding to 500 mL of bacterial culture were resuspended in 25 mL of buffer A (Tris HCl 20 mM, NaCl 200 mM, and EDTA 1 mM, pH 7.5) and sonicated. The suspension was

centrifuged for 30 min at 12,000 g to remove cell debris, and the supernatant was incubated for 24 hours at 10°C with 0.75 mg of purified S219V-TEV-Arg_8 protease [52] to process the MBP-TEV-pepN-His fusion protein.

A HisTrap HP 1 mL column (GE Healthcare Life Sciences, Chicago, IL, USA) was equilibrated in Buffer A, and the digested supernatant was loaded on the column. After washing, proteins were eluted using buffer A supplemented with 200 mM imidazole. The eluted samples were pooled and extensively dialyzed against PBS buffer, and the protein concentrations were measured by the bicinchoninic acid method.

3. Results and discussion

3.1. Synthesis

Synthesis of DCM–NH–Ala was accomplished through a simple two-step route starting from ICT derivative **1**, which was prepared as previously described by Sun *et al*. [21]. The reaction of the aniline derivative with commercially available N-Boc-Alanine provided the corresponding amide, which was transformed into DCM–NH–Ala after deprotection of the *tert*-butoxycarbonyl group by treatment with trifluoroacetic acid (see the SI for more details on the synthesis and characterization).

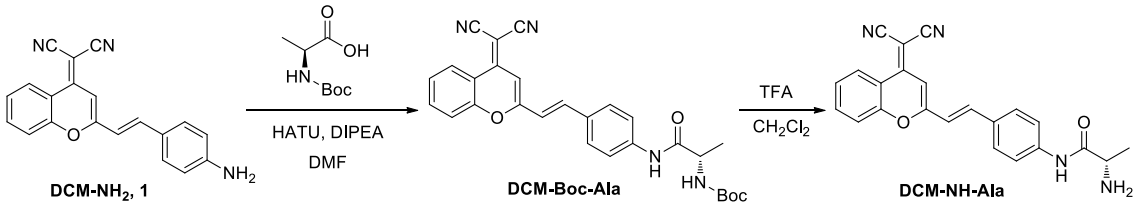

Scheme 1. Synthesis of DCM–NH–Ala.

3.2. Photophysical characterization of the enzymatic reaction

The absorption spectra of DCM–NH_2 and DCM–NH–Ala in the PBS/DMSO (7/3, v/v), 50 mM, pH = 7.4 solution are shown in Fig. 1A. The DCM–NH–Ala spectrum shows an ITC broad absorption band at 444 nm ($\varepsilon = 1.72 \times 10^4$ L mol^{-1} cm^{-1}), while the band from DCM–NH_2 has an absorption maximum at 480 nm ($\varepsilon = 3.77 \times 10^4$ L mol^{-1} cm^{-1}). The corresponding emission spectra are shown in Fig. 1B; the DCM–NH–Ala spectrum shows a weak emission band (λ_{ex} = 440 nm) with a maximum around 571 nm (Φ = 0.0009), and the DCM-NH_2 spectrum shows an intense emission band (λ_{ex} = 488 nm) with a maximum at 662 nm (Φ = 0.0063). The use of a 30% DMSO solution with this dye is common to prevent auto-quenching due to π-stacking [31]. To further investigate the minimum amount of DMSO before auto-quenching, we measured the fluorescence intensity at 662 nm (λ_{ex} = 458 nm and 480 nm) from solutions of free DCM–NH_2 with different DMSO percentages (Fig. S2). As can be seen, the fluorescence signals decreased when less than 30% DMSO was used, and in addition, the dye precipitated shortly after dissolving. In a deeper solvatochromic study of

DCM–NH_2, the quantum yields and fluorescence lifetimes of 12 different solvents are reported in the SI (see Fig. S3). A careful analysis of all the spectra using the Catalan approach shows that the parameter that exhibits the most drastic effects on the absorption spectra is solvent basicity, although polarity also has an influence. In contrast, the parameters that affect the emission spectra more are dipolarity and acidity (see Table S1 in the SI for more information)

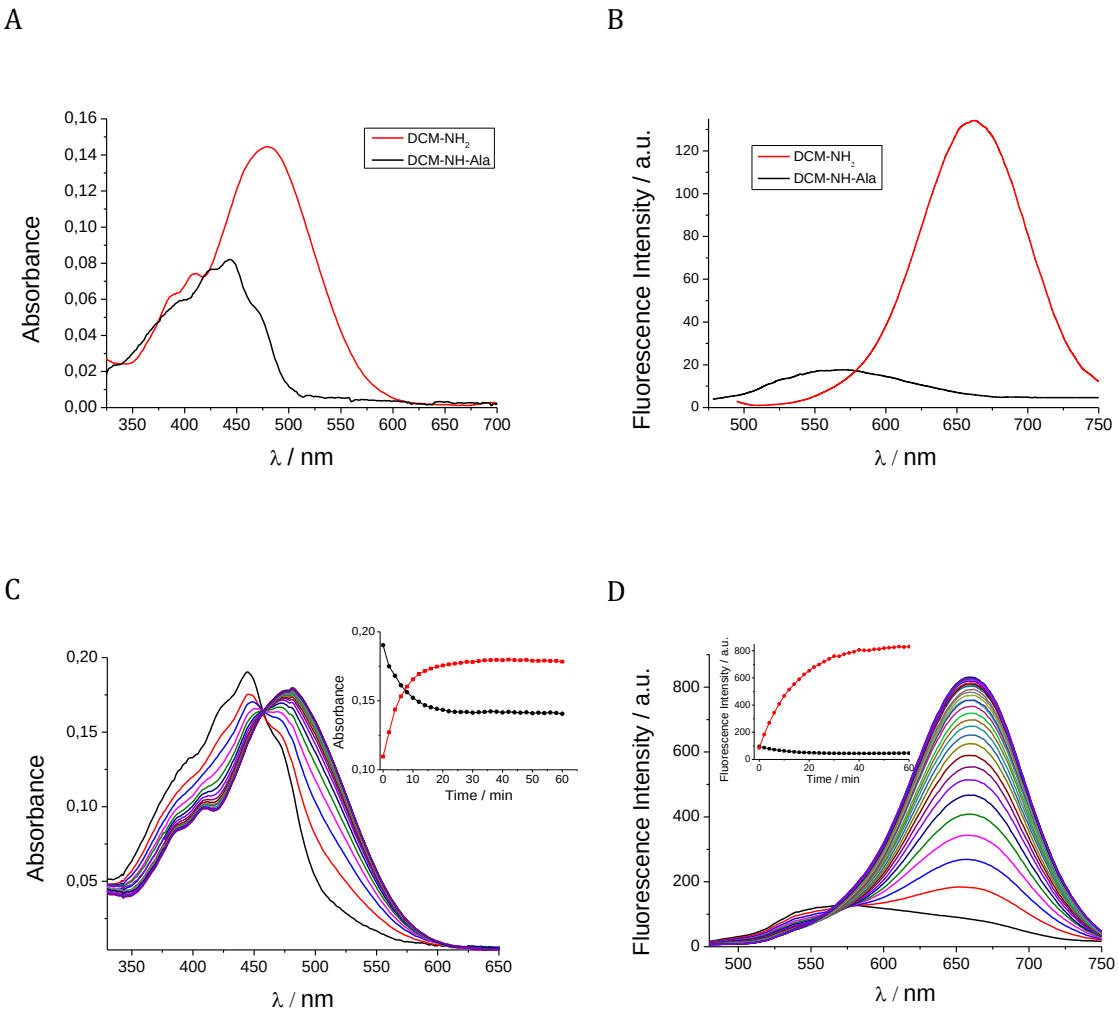

Figure 1. A) Absorption spectra of the pure compounds DCM–NH–Ala (red line) and DCM–NH_2 (black line) at approximately 4 µM. b) Emission spectra of the pure compounds DCM–NH–Ala (black line) and DCM–NH_2 (red line) at approximately 4 µM by excitation at 440 nm and 480 nm, respectively. C) Evolution of the absorption spectra of DCM–NH–Ala (10 µM) with pepN (10 µg/mL) every 2 minutes for 1 hour at T=37°C. The inset shows the maximum absorbance values at 480 nm (black line) and 444 nm (red line) vs time. D) Evolution of the emission spectra of DCM–NH–Ala (10 µM) with pepN (10 µg/mL) observed every 2 minutes for 1 hour by excitation at 458 nm at T=37°C. The inset shows the maximum fluorescence intensity at 662 nm (red line) and the intensity decrease at 540 nm (black line) vs time.

The addition of purified pepN to the DCM–NH–Ala 10 mM in DMSO/PBS (3/7, v/v), 10 mM, and pH = 7.4 solution resulted in a decrease in the absorption band with λ_{max} = 444 nm, which corresponds to the alanine derivative, along with a concomitant increase of a broad absorption band with a maximum at 480 nm, which is attributed to DCM-NH_2 (Fig. 1C), and gives rise to an isosbestic point at 458 nm. Correspondingly, the emission spectra of the solutions when excited at the isosbestic point show the strongest decrease at 540 nm (the intensity at the DCM-Ala maximum –571 nm– shows a slight decrease followed of an increase due to the influence of the strong emission from the released DCM-NH_2. See Fig. S4A) and the simultaneous sharp increase of the band with peak at 662 nm. As can be observed, both the absorption and emission spectra that appear after adding the enzyme are coincident with those shown by free DCM-NH_2. Importantly, the ratios between these both fluorescence signals I_{662}/I_{540} achieve the highest sensitivity increasing by 13 times after 20 minutes and by 18 times after 40 minutes due to the addition of alanine amino peptidase, and they remained constant after this time (see Fig. S4B).

To unambiguously determine that the increases in the aforementioned fluorescence ratios were induced by pepN activity, different concentrations of the specific inhibitor bestatin were mixed to substrate solutions of the same concentration, and the enzyme was then added. In Fig. 2A and 2C, the absorption and fluorescence spectra from those solutions are displayed. The absorption and emission spectra were acquired every 5 minutes. The absorption spectra showed a rapid rate of release when bestatin was absent (upper left panel in Fig. 2A); however, the addition of the inhibitor produced a decrease in the appearance of the red band (λ = 480 nm) that corresponded with the DCM-NH_2 released and was dependent on the bestatin concentration (upper right, left and right lower panels in Fig. 2A). In Fig. 2B we recovered the absorbance values at λ = 480 nm from the panels in Fig. 2A.

Similar to absorbance, the panels in Fig. 2C show that the fluorescence signal at 662 nm is diminished in the presence of the pepN inhibitor. This decrease is dependent on the bestatin concentration. In the upper left panel, a rapid appearance of the peak at 662 nm is observed, which is associated with the DCM-NH_2 released. The incorporation of bestatin slows the reaction rate and produces a decrease of the 662 nm peak at the same time point. As bestatin barely affects the emission of DCM-NH_2, the significant NIR fluorescent band peak at 662 nm must be attributed to the DCM-NH_2 released by specific amide bond cleavage because of pepN activity.

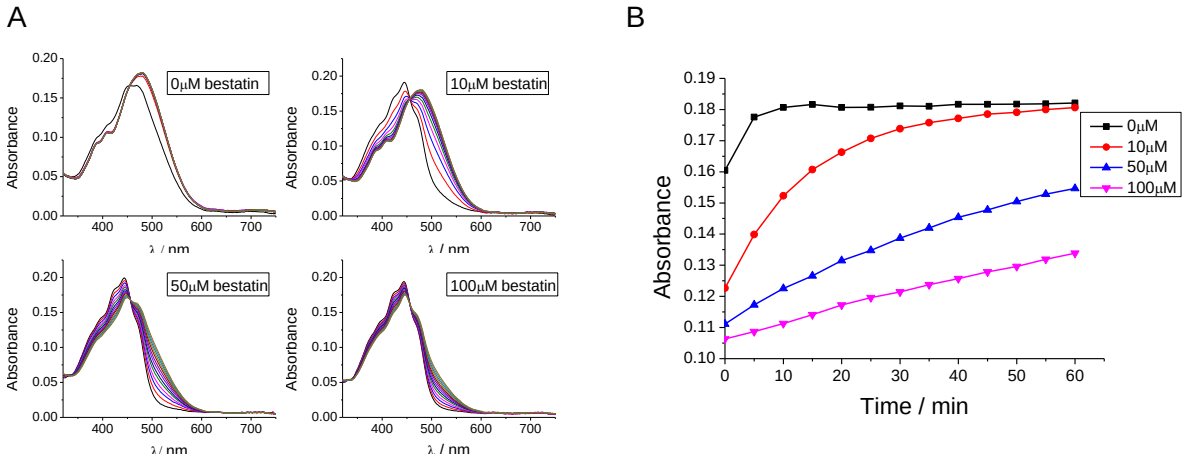

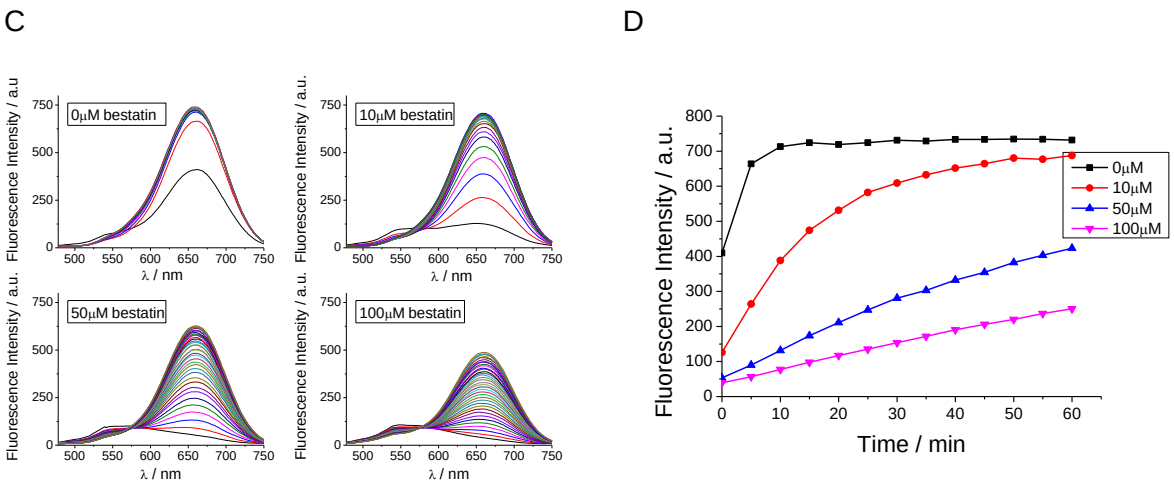

Figure 2. A) Absorption spectra of DCM−NH−Ala (10 μM) in the presence of alanine aminopeptidase (5 μg/mL) and bestatin at different concentrations for 1 hour. B) Representation of the absorbance at λ= 480 nm vs time for the different probe solutions (DCM−NH−Ala) with alanine aminopeptidase at different bestatin concentrations. C) Emission spectra of DCM−NH−Ala (10 μM) in the presence of alanine aminopeptidase (5 μg/mL) and bestatin at different concentrations for 1 hour with excitation at λ= 458 nm. D) Representation of emissions at the maximum λ=662 nm vs time the different probe solutions (DCM−NH−Ala) with alanine aminopeptidase for the different concentrations of bestatin.

According to Fig. 1C the maximum concentration of DCM−NH_2 was reached after approximately 20 minutes and the increase in time to a considerably higher value (t=∞) did not provide a concentration of DCM−NH_2 equivalent to the initially added substrate. We believe this result is due to the effects of DMSO on the protein structure. Since the effects caused by DMSO are different for each protein [53], to establish the effects of a 30% concentration of DMSO on the action of pepN, we performed an experiment in which 0.15 mL of substrate was added to either 1.5 mL of enzyme dissolved in PBS or to the same 1.5 mL of enzyme that had previously been incubated for 20 minutes in DMSO/PBS 3/7. The fluorescence spectra from each solution were recorded at different times, which allowed a comparison of the speeds at which the enzyme generated the reaction product in both samples. The recorded spectra are presented in Figs. S5, S6 and S7, in which it can be clearly seen that DMSO barely affected the initial rate of the enzymatic reaction. In addition to this, after 25 minutes a similar signal was reached in both solutions. In light of these results, we concluded that using solutions with 30% DMSO to conduct in vitro studies would not produce substantial errors in the parameters that describe the enzyme-substrate reaction but was necessary for adequate probe solubility. Moreover, we checked the efficiency of the enzyme activity at different pH levels (Fig. S8).

3.3. Kinetic parameters according to the Michaelis-Menten model

Since both species, DCM−NH_2 and DCM−NH−Ala, are excited at the wavelength of the isosbestic point, the ratiometric signal I_{662}/I_{540} is not a direct measurement of the free dye released by the enzymatic reaction, and therefore, corrections based on the molar extinction coefficients and quantum yields of both species must be made to achieve an

accurate value for the initial rate of the enzymatic reaction. To avoid making these corrections, the solutions used to calculate the characteristic parameters of the reaction kinetics were excited at a wavelength at which the DCM–NH–Ala was practically not excited. As shown in Fig. 1C, excitation at 550 nm generates essentially equal emission spectra regardless of the relative amounts of substrate and product in the solution at different reaction times. Therefore, excitation at 550 nm generates fluorescence signals that are proportional to the concentration of the reaction product without needing any corrections.

Considering the above information, we studied the enzyme kinetics following the Michaelis-Menten model. To resolve the kinetics, the initial rates of the enzymatic reaction at different initial substrate concentrations were calculated from the fluorescence signal produced by DCM–NH_2 (Fig S9). By using experimental nonlinear fitting between the fluorescence intensity and the quantity of DCM–NH_2 released (Fig. S10), we transformed this parameter into the concentration of the reaction product. Finally, Michaelis-Menten nonlinear regression fitting by least squares provided the K_M, v_{max} and $k_{catalytic}$ values listed in Table 1 (see SI, Fig. S11). As a reference, we measured the same parameters with a colorimetric method using L-alanine-4-nitroanilide hydrochloride as the substrate. The K_M value obtained from this method was higher than that obtained with DCM–NH–Ala and thus indicated that for the experimental conditions used, DCM–NH–Ala had a stronger affinity for the active enzyme site. However, the $k_{catalytic}$ of DCM-Ala was significantly lower than that of the colorimetric substrate. These results suggest that the high affinity of pepN for DCM–NH–Ala also translates to a DCM–NH_2 output kinetic constant (k_{off}) from the active site that probably slows the reaction rate. This difference could be enhanced by the use of DMSO for DCM–NH–Ala in the reaction media. Although the use of this cosolvent has been reported to produce a slight loss of enzyme rigidity and provide higher substrate penetrability and therefore a decreasing K_M, the loss of rigidity can also cause a slight impairment in its efficiency and decreases $k_{catalytic}$. Similar effects have been reported previously for other enzymes [54, 55]. Moreover, we also measured the DCM–NH–Ala and DCM–NH_2 emissions excited at the isosbestic point at different substrate concentrations. Although the ratios cannot be used to calculate the kinetic parameters, the results confirm that ratiometric measurements can be used as signals to monitor pepN activity (Fig S12).

Table 1.

	Substrate	
	DCM-Ala	L-alanine-4-nitroanilide hydrochloride
K_M	0.082 ± 0.021 mM	0.68 ± 0.04 mM
v_{max}	(4.8 ± 0.8) × 10^{-3} mM min^{-1} mg^{-1}	(7.3 ± 0.1) × 10^{-3} mM min^{-1} mg^{-1}
$k_{catalytic}$	0.47 ± 0.08 mM min^{-1} μM^{-1}	0.72 ± 0.01 mM min^{-1} μM^{-1}

3.4. Ratiometric monitoring of endogenous pepN activity in bacteria.

Once the photophysical characteristics of the enzymatic reaction between DCM–NH–Ala and alanine aminopeptidase were determined in vitro and given that the

purpose of this research was to develop a new methodology for identifying of Gram (−) bacteria that express pepN activity, the probe performance in bacteria was explored by both one-photon and two-photon fluorescence microscopy while considering the excellent biocompatibility that DCM-NH_2 has shown in previous studies of living cells [45].

E. coli was selected as the bacterial model. For the assays, two clones were selected. First, as a control bacteria, XL1-blue cells transformed with a GFPuv encoding plasmid were used. In these bacteria, a basal level of pepN activity was detected. In addition, GFP fluorescence allows these bacteria to be differentiated from others. The second clone used corresponded to XL1-blue competent cells transformed with the pMAL-TEV-pepN-His plasmid. In these bacteria, increased expression of the pepN gene product could be detected without the addition of IPTG as an inductor due to the leakage of the expression plasmid [56]. Finally, a third group of samples was that in which bacteria harboring the pMAL-TEV-pepN-His plasmid were induced with IPTG to enhance pepN activity.

Because bacteria have great mobility, in these experiments we immobilized them by placing low melting point agarose gel containing DCM−NH−Ala (10 μM) on an aliquot of bacterial culture. Next, the gels were placed on a microscope and were excited by two photons of 800 nm light, and fluorescence was recorded in both the green and red channels. Fig. 3 shows images of bacteria at four discrete times along with the representative fluorescence of the red channel at each recorded minute for the three *E. coli* strains. As a control, we incorporated *E. coli* bacteria that express GFP to both quickly focus the microscope at zero time and to more clearly observe the temporal evolution of the fluorescence intensity emitted in the red channel; a video (v1, see the Supplementary Data) is also attached to this manuscript that shows the temporal evolution of the emitted red fluorescence. For this reason, it should be noted that in this figure, the fluorescence in the green channel was suppressed because green emissions from *E. coli* bacteria that express GFP can significantly modify the ratio calculations around their locations. Moreover, GFP was useful to identify bacteria that overexpressed (or not) pepN. In fact, the bacteria that overexpress pepN display a red signal whose intensity is twice that corresponding to bacteria with inhibited pepN expression and ten times greater than the signal intensity of bacteria that lack this plasmid (e.g., GFP expressing bacteria). Therefore, the emission appearance kinetics are dependent on the intracellular pepN concentrations. All of these results indicate that the probe spontaneously penetrates Gram (−) bacteria and is capable of revealing with great sensitivity the presence of pepN inside bacteria by using the emitted fluorescence after excitation with two 800 nm photons. At this point, it should be highlighted that the advantage of being able to detect different expression of pepN provides a powerful tool to detect various virulent bacterial agents and allows discrimination among different pathogenic microorganisms.

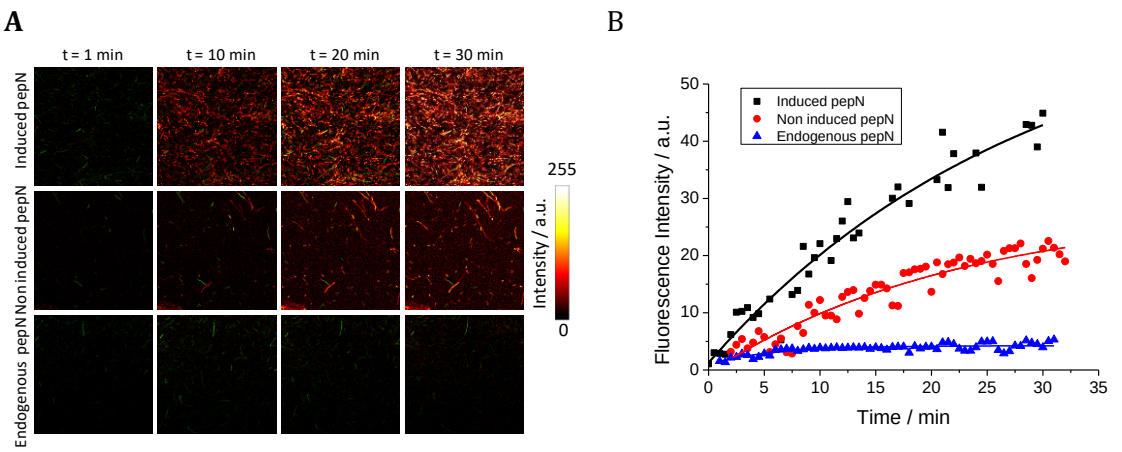

Figure 3. Images of different types of bacteria incubated with DCM–NH–Ala (5 μM) that were taken at different times using multiphoton microscopy (λ_{ex} = 800 nm). B) Representation of the fluorescence intensity in the red channel (λ_{em} = 580-700 nm) of the different bacterial strains at different times.

To unquestionably demonstrate that the NIR emissions are due to DCM-NH_2 released by the enzymatic reaction of the intrabacterial pepN, *E. coli* from the pepN overexpressed strain were preincubated in the presence or absence of the competitive inhibitor bestatin (0.5 mM, 10 minutes) and then with DCM–NH–Ala 10 μM in DMSO/PBS (3/7, v/v), pH 7.4 for 30 minutes (Fig. 4).

As can be observed, *E. coli* strains with pepN activity exhibit a decreasing fluorescence signal in the green channel along with a concomitant increase of the NIR fluorescence signal in the red channel, which is consistent with the spectral changes observed *in vitro* and therefore in their red:green ratios, are shown in Fig. 4A. However, Fig. 4B shows that the bacteria incubated in the presence of bestatin show a considerable reduction in the increase in NIR fluorescence due to DCM–NH_2 release and exhibit a 4-fold decrease in the ratiometric signal; this finding convincingly demonstrates that the formation of DCM–NH_2 is caused by the enzymatic activity of pepN. For a better comparison, the mean values of bacteria from these two strains are shown in Fig. 4C.

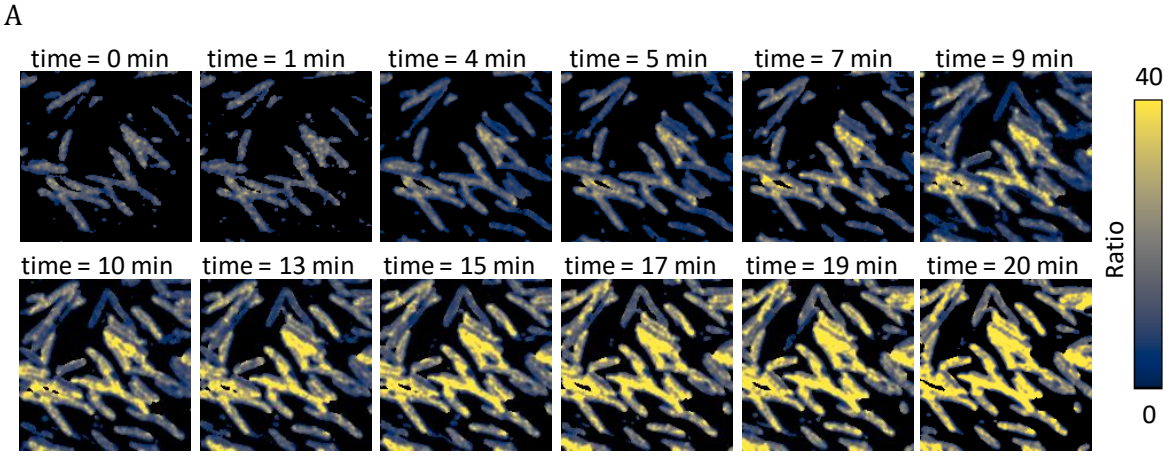

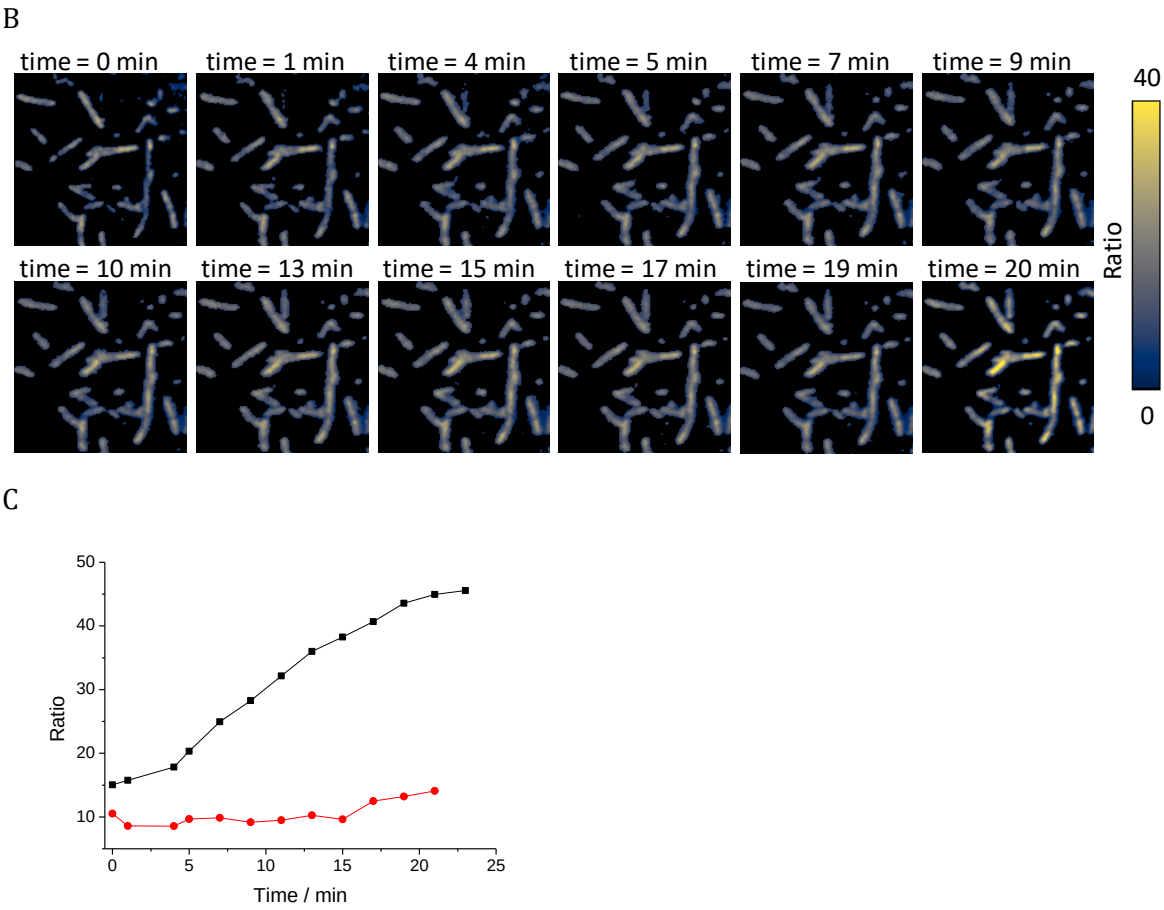

Figure 4. A) Ratiometric images of the *E. coli* strain with pepN induced at different times B) The same *E. coli* strain after incubation with bestatin (0.5 mM) at different time points C) Representation of the ratios of both the control (induced pepN bacteria) and bacteria with bestatin at different times.

Multiphoton microscopy allows three-dimensional *in vivo* microscopy in scattering materials with a submicron resolution and a high signal-to-noise ratio. As infections with Gram (−) microorganisms can occur in deep tissues, we performed experiments to compare the results obtained by excitation with two 800 nm photons or by only one 458 nm photon. Thus, quantification of the fluorescence background from the scattering materials and the increase in the depth of penetration in these materials could be calculated. To simulate absorption from biological materials [57], instead of the usual culture media used in the growth of bacterial strains, we used an agar medium enriched with 15% lysogeny broth (LB). The results obtained at three different Z-positions are shown in Fig. 5. Panel A shows images recorded in the wavelength range between 580 and 700 nm at three different arbitrary Z-positions from *E. coli* grown in agar medium that was extra-enriched with LB 15% and excited by either one photon of 458 nm wavelength or two photons of 800 nm wavelength. For better visualization, panel B shows a zoomed image (left image) with two extra-zoomed squares indicated. In panel C, the mean intensity of the red channel and relative intensity value (normalized by the maximum) between the images from the two-photon and one-photon excitations obtained every 3 μm are shown. It is evident that the intensity of the fluorescence emitted when the sample is excited with a single 458 nm photon is less than that of when it is excited by two 800 nm photons. Moreover, both

intensities decrease when the relative value of Z_r increases, although the decrease is more pronounced at increased depths when excited by a photon. At Z_r = 210 µm, the fluorescence from excitation by one 458 nm photon nearly disappears completely. Moreover, another important advantage of two-photon excitation is the increased signal-to-noise ratio due not only to the improved signal but also to the decrease in noise. Fig. 5D shows three different images at three arbitrary Z_r positions. In this analysis, we generated an intensity plot profile from the three segments indicated in the images, which is shown in panel B. When a segment crosses a bacteria cell, it corresponds with a peak in the intensity profile. The upper, medium and lower profiles correspond to segments one, two and three, respectively. Profiles from the two-photon excitation images are represented by the black color, and those from one-photon excitation are shown in red. As shown in Fig. 5, the signal from the two-photon excitation is more intense than that which corresponds to excitation with one photon. However, in addition, the noise level observed in the two-photon excitation is significantly lower. Therefore, the combination of our probe with this technique provides a notable improvement in the determination of the pepN activity in tissues or *in vivo*.

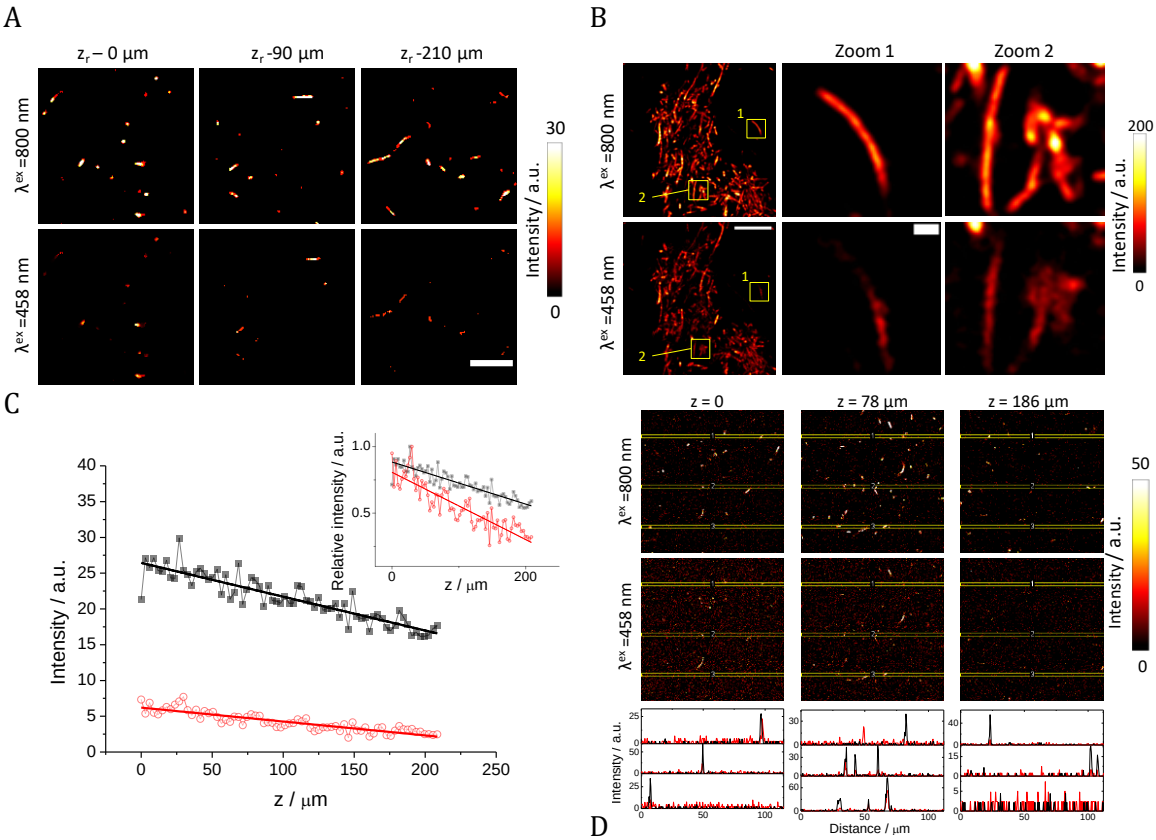

Figure 5. A) Images of *E. coli* obtained in an agar medium extra-enriched with LB 15% ($\lambda_{acquisition}$ = 580-700 nm) at two different wavelengths for λ_{ex} = 800 nm (upper panel) and 458 nm (lower panel) at three different z-positions. The first column indicates the relative z=0, the second column indicates the increase in depth to 90 µm and the third column indicates the increase in depth to 210 µm. The bar length corresponds to 100 µm. B) Zoomed *E. coli* images. In the first column, the bar length corresponds to 20 µm and the two squares indicated are extra-zoomed in the middle and right columns. The bar lengths in the extra-zoomed images represent 2 µm C) Intensity means of the red channel (λ acquisition = 580-700 nm) from a bacterial culture immersed in LB medium (15%) at different z positions. The inset shows the

decrease in the relative intensity between the images from two-photon excitation (squares, λ_{ex} = 800 nm) and one-photon excitation (circles, λ_{ex} = 458 nm). All images were obtained after 30 minutes of incubation with DCM−NH−Ala to ensure the presence of DCM-NH_2. D) Images obtained of *E. coli* in an agar medium extra-enriched with LB 15% ($\lambda_{acquisition}$ = 580-700 nm) at wavelengths of λ_{ex} = 800 nm (upper panel) and 458 nm (lower panel) at three different z-positions. The lower panel shows the intensity profile of the red channel for the three marks indicated in the upper panel at λ_{ex} = 800 nm (black lines) and λ_{ex} = 458 nm (red lines) at three different z positions.

To obtain a good resolution in STED microscopy, it is essential to achieve a good signal-to-noise ratio [16]. In this sense, it is important to record enough fluorescent photons from the fluorescent subdiffraction regions, and therefore, high brightness and photostability of the fluorophore are essential requirements for application as a STED nanoscopy probe. One of the drawbacks for the applicability of STED probes for many fluorophores with adequate photophysical properties is that they are not permeable to the cell membrane and therefore are not appropriate for labeling living organisms since it is necessary to wash samples to avoid background fluorescence. Thus, it is necessary to find new useful fluorophores as STED probes in living organisms that do not need a washing step.

To demonstrate that DCM−NH_2 meets the requirements for use as an effective probe in super-resolution microscopy, we added a probe solution (500 μM in DMSO/PBS (3/7, v / v) pH 7.4) to an *E. coli* bacteria culture to achieve a final concentration of 5 μM and then immediately made the measurements. Fig. 6A (and Fig. S13) show that the fluorophore quickly enters the bacterial body and is selectively accumulated on the bacterial membrane, which corresponds to the apolar character of the probe. In addition, points of greater intensity, which probably correspond to regions of higher lipophilia and reflect the heterogeneity of the membrane, are also observed. We compare the confocal and STED images in Fig. 6A, in which the plot profiles of both images are shown and which unambiguously demonstrate the usefulness of the fluorophore in STED nanoscopy. Next, we performed the following experiment to observe the dynamics of enzymatic reactions in strains of bacteria with induced and endogenous pepN that were incubated with a DCM−NH−Ala solution. The images shown in Fig. 6B were collected at 5, 15 and 35 minutes. From the set of results shown in Fig. 6B, with respect to the induced pepN strain, it appears that the probe quickly initiated the enzymatic reaction at specific sites located on the bacterial membrane and in some structures within the bacterial body (see Fig. 6C, Fig. S14 and video v2, see Supplementary Data), and then, the released dye diffused. Similar to the behavior with DCM−NH_2, the released compound accumulated in the bacterial membrane due to its lipophilic nature. In contrast, the endogenous pepN strain showed a slower increase in fluorescence and the release was also focused in the membranes. Therefore, the rapid enzymatic reactions were not present in the internal structures.

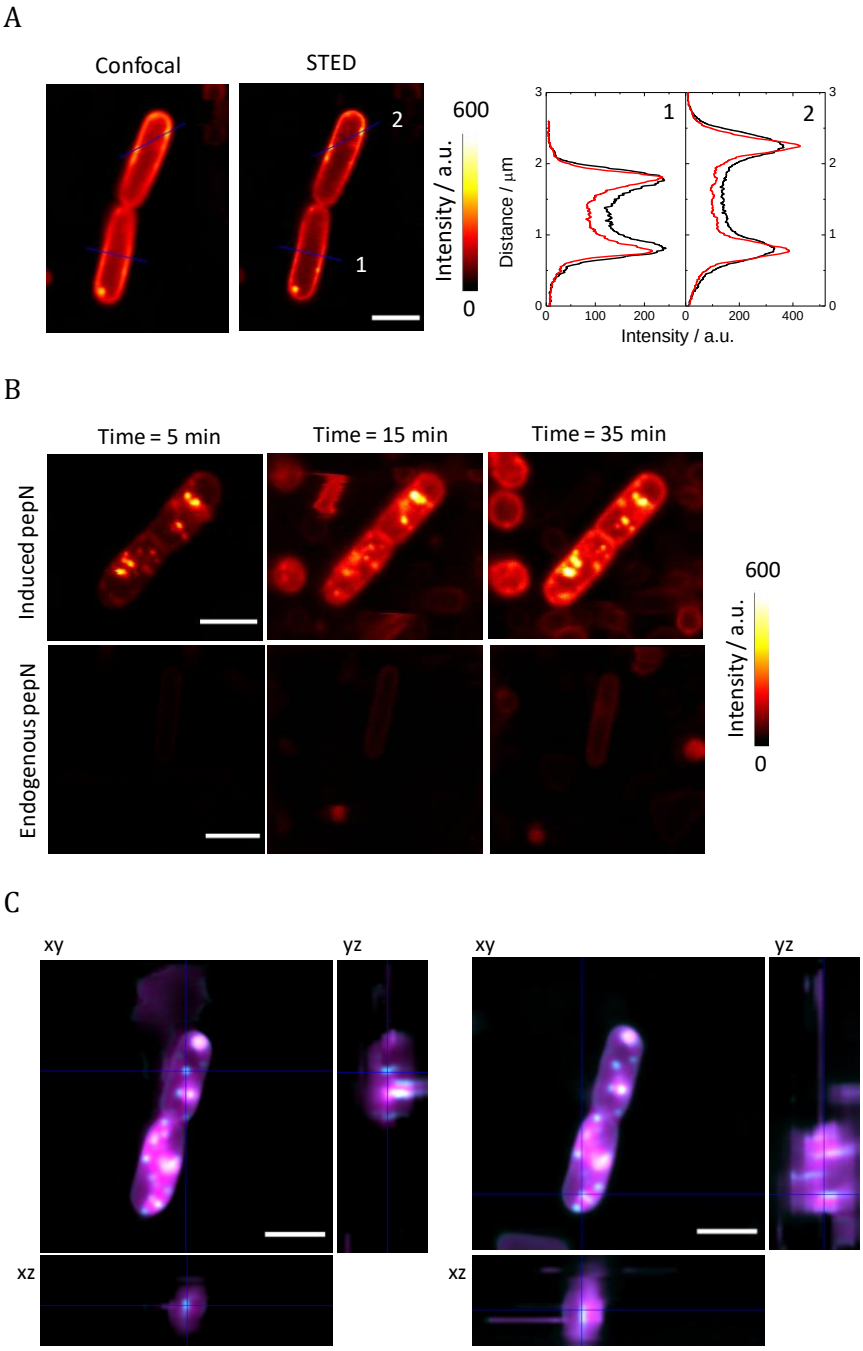

Figure 6. A) Images obtained from *E. coli* using confocal and STED microscopy. Graphs represent the plot profile (black corresponds to confocal images and red to STED images) for lines 1 and 2 shown in the images. B) STED images of the *E. coli* strain with pepN induced (upper line) and with endogenous pepN (lower line) at different times. C) xy images obtained from *E. coli* (square images) in different z-planes (yz and xz, rectangular images). The bacterial bodies are colored in magenta and the structures where the increase in fluorescence is high are colored in cyan/white. The crosses mark the structures that are not attached to the bacterial membrane. The scale bars represent 2 µm.

The interest in the detection of alanine peptidase in identifying Gram (−) pathogenic bacteria has led to the synthesis of several colorimetric and fluorometric probes. Thus, fluorogenic substrates have been synthesized [58], as well as fluorophores that display a considerable wavelength shift before and after the reaction with the enzyme [59]. A probe has recently been proposed that takes advantage of the blue-to-yellow fluorescent transition when the enzymatic reaction occurs [60]. The probe proposed here has the advantages over the aforementioned of its emission in the red and the possibility of excitation by two NIR photons, obviating the possible autofluorescence of the medium as well as increasing the penetration both in the culture media and in the tissues. Moreover, its exceptional fluorescence has allowed its use in super-resolution microscopy.

4. Conclusions

In this paper, we present a specific substrate, DCM−NH−Ala, that causes a sharp increase in the fluorescence band with peak at 662 nm when excited by a single photon at 480 nm or by two NIR photons (at approximately 800 nm) via an enzymatic reaction with alanine amino peptidase. Taking advantage of the biocompatibility that the probe has shown with living organisms, a new methodology for identifying of Gram (−) bacteria that express pepN activity is proposed. The emission appearance kinetics are dependent on the intracellular pepN concentrations and represent a powerful tool for detecting various virulent bacteria agents in a few minutes and have the inherent advantages of two-photon excitation. In addition, the released fluorophore DCM−NH_2 meets the requirements for use as an effective probe in super-resolution microscopy. As indicated by the results obtained, the probe quickly initiates enzymatic reactions at specific sites located on the bacterial membrane and in some structures within the bacterial body; the released dye then diffuses and accumulates in the bacterial membrane due to its lipophilic nature.

Declaration of Competing Interest

There are no conflicts to declare.

Acknowledgements

This work was financially supported by CTQ2017-85454-C2-1-P, CTQ2017-86125-P and CTQ2017-85658-R (MICIU/AEI/ERDF). JVP is supported by a FPU fellowship (FPU17/04749). CSG was supported by a Research initiation grant (Plan Propio 2018, University of Granada, Spain). We acknowledge the Universidad de Granada (Spain) microscopy central facilities (CIC-UGR).

Appendix A. Supplementary data

The following are supplementary data for this article:

- Supporting Information doc.
- Video v1
- Video v2

References

[1] H. Kobayashi, M. Ogawa, R. Alford, P.L. Choyke, Y. Urano, New Strategies for Fluorescent Probe Design in Medical Diagnostic Imaging, Chem. Rev., 110(2010) 2620-40.
[2] Y. Koide, Y. Urano, K. Hanaoka, W. Piao, M. Kusakabe, N. Saito, et al., Development of NIR Fluorescent Dyes Based on Si-rhodamine for in Vivo Imaging, J. Am. Chem. Soc., 134(2012) 5029-31.
[3] E.A. Owens, M. Henary, G. El Fakhri, H.S. Choi, Tissue-Specific Near-Infrared Fluorescence Imaging, Acc. Chem. Res., 49(2016) 1731-40.
[4] L. Crovetto, A. Orte, J.M. Paredes, S. Resa, J. Valverde, F. Castello, et al., Photophysics of a Live-Cell-Marker, Red Silicon-Substituted Xanthene Dye, J. Phys. Chem. A, 119(2015) 10854-62.
[5] A.P. Gorka, R.R. Nani, M.J. Schnermann, Harnessing Cyanine Reactivity for Optical Imaging and Drug Delivery, Acc. Chem. Res., 51(2018) 3226-35.
[6] L.L. Wang, W. Du, Z.J. Hu, K. Uvdal, L. Li, W. Huang, Hybrid Rhodamine Fluorophores in the Visible/NIR Region for Biological Imaging, Angew. Chem. Int. Ed., 58(2019) 14026-43.
[7] W. Denk, J. Strickler, W. Webb, Two-photon laser scanning fluorescence microscopy, Science, 248(1990) 73-6.
[8] H.W. Liu, Y.C. Liu, P. Wang, X.B. Zhang, Molecular engineering of two-photon fluorescent probes for bioimaging applications, Methods Appl. Fluoresc., 5(2017) 012003.
[9] M. Göppert-Mayer, Über Elementarakte mit zwei Quantensprüngen, Ann. Phys., 401(1931) 273-94.
[10] H.M. Kim, B.R. Cho, Small-Molecule Two-Photon Probes for Bioimaging Applications, Chem. Rev., 115(2015) 5014-55.
[11] S. Yao, K.D. Belfield, Two-Photon Fluorescent Probes for Bioimaging, Eur. J. Org. Chem., 2012(2012) 3199-217.
[12] S.W. Hell, J. Wichmann, Breaking the diffraction resolution limit by stimulated emission: stimulated-emission-depletion fluorescence microscopy, Opt. Lett., 19(1994) 780-2.
[13] S.J. Sahl, S.W. Hell, S. Jakobs, Fluorescence nanoscopy in cell biology, Nat. Rev. Mol. Cell Biol., 18(2017) 685-701.
[14] S. Pujals, L. Albertazzi, Super-resolution Microscopy for Nanomedicine Research, ACS Nano, 13(2019) 9707-12.
[15] T. Muller, C. Schumann, A. Kraegeloh, STED Microscopy and its Applications: New Insights into Cellular Processes on the Nanoscale, ChemPhysChem, 13(2012) 1986-2000.
[16] G. Vicidomini, P. Bianchini, A. Diaspro, STED super-resolved microscopy, Nat. Methods, 15(2018) 173-82.
[17] B. Valeur, I. Leray, Design principles of fluorescent molecular sensors for cation recognition, Coord.Chem.Rev., 205(2000) 3-40.
[18] M.H. Lee, J.S. Kim, J.L. Sessler, Small molecule-based ratiometric fluorescence probes for cations, anions, and biomolecules, Chem. Soc. Rev., 44(2015) 4185-91.
[19] X.M. Wu, X.R. Sun, Z.Q. Guo, J.B. Tang, Y.Q. Shen, T.D. James, et al., In Vivo and in Situ Tracking Cancer Chemotherapy by Highly Photostable NIR Fluorescent Theranostic Prodrug, J. Am. Chem. Soc., 136(2014) 3579-88.
[20] J.L. Fan, W. Sun, Z.K. Wang, X.J. Peng, Y.Q. Li, J.F. Cao, A fluorescent probe for site I binding and sensitive discrimination of HSA from BSA, Chem. Commun., 50(2014) 9573-6.
[21] W. Sun, J.L. Fan, C. Hu, J.F. Cao, H. Zhang, X.Q. Xiong, et al., A two-photon fluorescent probe with near-infrared emission for hydrogen sulfide imaging in biosystems, Chem. Commun., 49(2013) 3890-2.

[22] X.J. Song, C.C. Li, Y. Wang, D.H. Wang, Z.H. Liu, A ratiometric two-photon fluorescence probe for monitoring mitochondrial HOCl produced during the traumatic brain injury process, Sensor. Actuat. B-Chem., 311(2020) 127895.
[23] X.J. Zhao, C. Wang, G.Q. Yuan, H.Y. Ding, L.Y. Zhou, X.G. Liu, et al., A dual-site modulated FRET-based two-photon ratiometric fluorescent probe for tracking lysosomal pH changes in living cells, tissues and zebrafish, Sensor. Actuat. B-Chem., 290(2019) 79-86.
[24] W. Hu, L.Y. Zeng, S.Y. Zhai, C.C. Li, W.Q. Feng, Y. Feng, et al., Developing a ratiometric two-photon probe with baseline resolved emissions by through band energy transfer strategy: Tracking mitochondrial SO2 during neuroinflammation, Biomaterials, 241(2020) 119910.
[25] G. Cerny, Studies on the aminopeptidase test for the distinction of gram-negative from gram-positive bacteria, Eur. J. Appl. Microbiol. Biotechnol., 5(1978) 113-22.
[26] F.C. Golich, M. Han, M.W. Crowder, Over-expression, purification, and characterization of aminopeptidase N from Escherichia coli, Protein Expr. Purif., 47(2006) 634-9.
[27] M. Potempa, J. Potempa, Protease-dependent mechanisms of complement evasion by bacterial pathogens, Biol. Chem., 393(2012) 873-88.
[28] M.A. DeJesus, E.R. Gerrick, W.Z. Xu, S.W. Park, J.E. Long, C.C. Boutte, et al., Comprehensive Essentiality Analysis of the Mycobacterium tuberculosis Genome via Saturating Transposon Mutagenesis, mBio, 8 (1) (2017) e02133-16.
[29] R.A. McAdam, S. Quan, D.A. Smith, S. Bardarov, J.C. Betts, F.C. Cook, et al., Characterization of a Mycobacterium tuberculosis H37Rv transposon library reveals insertions in 351 ORFs and mutants with altered virulence, Microbiol-Sgm, 148(2002) 2975-86.
[30] N. Sharma, S. Aggarwal, S. Kumar, R. Sharma, K. Choudhury, N. Singh, et al., Comparative analysis of homologous aminopeptidase PepN from pathogenic and non-pathogenic mycobacteria reveals divergent traits, PLoS One, 14 (4) (2019) e0215123.
[31] C.N. Nganje, S.A. Haynes, C.M. Qabar, R.C. Lent, E.N.B. Ghanem, M.G. Shainheit, PepN is a non-essential, cell wall-localized protein that contributes to neutrophil elastase-mediated killing of Streptococcus pneumoniae, PLoS One, 14(2019).
[32] C. Li, A targeted approach to cancer imaging and therapy, Nat. Mater., 13(2014) 110-5.
[33] S.H. Wilkes, J.M. Prescott, The slow, tight-binding of bestatin and amastatin to aminopeptidases, J. Biol. Chem., 260(1985) 3154-62.
[34] P. Aemaimanan, N. Sattayasai, N. Wara-Aswapati, W. Pitiphat, W. Suwannarong, S. Prajaneh, et al., Alanine Aminopeptidase and Dipeptidyl Peptidase IV in Saliva of Chronic Periodontitis Patients, J. Periodontol., 80(2009) 1809-14.
[35] Y. Huang, Y. Qi, C.Y. Zhan, F. Zeng, S.Z. Wu, Diagnosing Drug-Induced Liver Injury by Multispectral Optoacoustic Tomography and Fluorescence Imaging Using a Leucine-Aminopeptidase-Activated Probe, Anal. Chem., 91(2019) 8085-92.
[36] X.J. Liu, Q.Y. Zhang, F.L. Wang, J.H. Jiang, A near infrared fluorescent probe for the detection and imaging of prolyl aminopeptidase activity in living cells, Analyst, 144(2019) 5980-5.
[37] S.L. Huang, Y.L. Wu, F. Zeng, J.J. Chen, S.Z. Wu, A turn-on fluorescence probe based on aggregation-induced emission for leucine aminopeptidase in living cells and tumor tissue, Anal. Chim.Acta, 1031(2018) 169-77.
[38] M.Y. Hu, L. Li, H. Wu, Y. Su, P.Y. Yang, M. Uttamchandani, et al., Multicolor, One- and Two-Photon Imaging of Enzymatic Activities in Live Cells with Fluorescently Quenched Activity-Based Probes (qABPs), J. Am. Chem. Soc., 133(2011) 12009-20.
[39] L. Li, J.Y. Ge, H. Wu, Q.H. Xu, S.Q. Yao, Organelle-Specific Detection of Phosphatase Activities with Two-Photon Fluorogenic Probes in Cells and Tissues, J. Am. Chem. Soc., 134(2012) 12157-67.
[40] D. Kim, S. Sambasivan, H. Nam, K.H. Kim, J.Y. Kim, T. Joo, et al., Reaction-based two-photon probes for in vitro analysis and cellular imaging of monoamine oxidase activity, Chem. Commun., 48(2012) 6833-5.

[41] L. Li, C.W. Zhang, G.Y.J. Chen, B.W. Zhu, C. Chai, Q.H. Xu, et al., A sensitive two-photon probe to selectively detect monoamine oxidase B activity in Parkinson's disease models, Nat. Commun., 5(2014) 3276.
[42] S.Y. Yan, R. Huang, C.C. Wang, Y.M. Zhou, J.Q. Wang, B.S. Fu, et al., A Two-photon Fluorescent Probe for Intracellular Detection of Tyrosinase Activity, Chem. Asian J., 7(2012) 2782-5.
[43] H. Zhang, J.L. Fan, J.Y. Wang, S.Z. Zhang, B.R. Dou, X.J. Peng, An Off-On COX-2-Specific Fluorescent Probe: Targeting the Golgi Apparatus of Cancer Cells, J. Am. Chem. Soc., 135(2013) 11663-9.
[44] H.W. Lee, C.H. Heo, D. Sen, H.O. Byun, I.H. Kwak, G. Yoon, et al., Ratiometric Two-Photon Fluorescent Probe for Quantitative Detection of beta-Galactosidase Activity in Senescent Cells, Anal. Chem., 86(2014) 10001-5.
[45] K.Z. Gu, Y.J. Liu, Z.Q. Guo, C. Lian, C.X. Yan, P. Shi, et al., In Situ Ratiometric Quantitative Tracing of Intracellular Leucine Aminopeptidase Activity via an Activatable Near-Infrared Fluorescent. Probe, ACS Appl. Mater. Interfaces, 8(2016) 26622-9.
[46] Y. Wang, L.W. Zhang, L.X. Chen, Glutathione Peroxidase-Activatable Two-Photon Ratiometric Fluorescent Probe for Redox Mechanism Research in Aging and Mercury Exposure Mice Models, Anal. Chem., 92(2020) 1997-2004.
[47] H.D. Li, Y.Q. Li, Q.C. Yao, J.L. Fan, W. Sun, S. Long, et al., In situ imaging of aminopeptidase N activity in hepatocellular carcinoma: a migration model for tumour using an activatable two-photon NIR fluorescent probe, Chem. Sci., 10(2019) 1619-25.
[48] H. Li, Q. Yao, W. Sun, K. Shao, Y. Lu, J. Chung, et al., Aminopeptidase N Activatable Fluorescent Probe for Tracking Metastatic Cancer and Image-Guided Surgery via in Situ Spraying, J. Am. Chem. Soc., 142(2020) 6381-9.
[49] J. Schindelin, I. Arganda-Carreras, E. Frise, V. Kaynig, M. Longair, T. Pietzsch, et al., Fiji: an open-source platform for biological-image analysis, Nat. Methods, 9(2012) 676-82.
[50] M. Foglino, S. Gharbi, A. Lazdunski, Nucleotide-sequence of the pepn gene encoding aminopeptidase-n of Escherichia-Coli, Gene, 49(1986) 303-9.
[51] M. Torres, S. Uroz, R. Salto, L. Fauchery, E. Quesada, I. Llamas, HqiA, a novel quorum-quenching enzyme which expands the AHL lactonase family, Sci. Rep., 7(2017) 943.
[52] R.B. Kapust, J. Tozser, J.D. Fox, D.E. Anderson, S. Cherry, T.D. Copeland, et al., Tobacco etch virus protease: mechanism of autolysis and rational design of stable mutants with wild-type catalytic proficiency, Protein Eng., 14(2001) 993-1000.
[53] D.S.H. Chan, M.E. Kavanagh, K.J. McLean, A.W. Munro, D. Matak-Vinkovic, A.G. Coyne, et al., Effect of DMSO on Protein Structure and Interactions Assessed by Collision-Induced Dissociation and Unfolding, Anal. Chem., 89(2017) 9976-83.
[54] A.P. Demchenko, O.I. Rusyn, A.M. Egorov, V.I. Tishkov, The solvent effects on the kinetics of bacterial formate dehydrogenase reaction, Biochim. Biophys. Acta, 1039(1990) 290-6.
[55] H.J. Wiggers, J. Cheleski, A. Zottis, G. Oliva, A.D. Andricopulo, C.A. Montanari, Effects of organic solvents on the enzyme activity of Trypanosoma cruzi glyceraldehyde-3-phosphate dehydrogenase in calorimetric assays, Anal.Biochem., 370(2007) 107-14.
[56] G.L. Rosano, E.S. Morales, E.A. Ceccarelli, New tools for recombinant protein production in Escherichia coli: A 5-year update, Protein Sci., 28(2019) 1412-22.
[57] S.L. Jacques, Optical properties of biological tissues: a review, Phys. Med. Biol., 58(2013) R37-R61.
[58] L. Varadi, M.Y. Wang, R.R. Mamidi, J.L. Luo, J.D. Perry, D.E. Hibbs, et al., A latent green fluorescent styrylcoumarin probe for the selective growth and detection of Gram negative bacteria, Biorg. Med. Chem., 26(2018) 4745-50.
[59] M. Cellier, A.L. James, S. Orenga, J.D. Perry, G. Turnbull, S.P. Stanforth, The Synthesis of L-Alanyl and beta-Alanyl Derivatives of 2-Aminoacridone and Their Application in the Detection of Clinically-Important Microorganisms, PLoS One, 11(7) (2016) e0158378.
[60] L. Varadi, E.Y. Najib, D.E. Hibbs, J.D. Perry, P.W. Groundwater, A Selective, Dual Emission beta-Alanine Aminopeptidase Activated Fluorescent Probe for the Detection of

Pseudomonas aeruginosa, Burkholderia cepacia, and Serratia marcescens, Molecules, 24(2019) 3550.